J Mol Model (2006) 12: 653–664
DOI 10.1007/s00894-006-0111-5

ORIGINAL PAPER

Christopher A. Brown · Michael L. McKee

Rearrangements in icosahedral boranes and carboranes revisited

Received: 29 April 2005 / Accepted: 27 July 2005 / Published online: 30 June 2006

Abstract The structure, stability, and intermolecular rearrangements between *ortho*-, *meta*-, and *para*-$C_2B_{10}H_{12}$ and $B_{12}H_{12}^{2-}$ were investigated using the hybrid density functional B3LYP/6-31G(d) for vibrational frequencies, as well as B3LYP/6-311+G(2d,p) for single-point electronic energies. The general trends in free energies of rearrangement between *ortho*-$C_2B_{10}H_{12}$ to *meta*-$C_2B_{10}H_{12}$ and *meta*-$C_2B_{10}H_{12}$ to *para*-$C_2B_{10}H_{12}$ presented here are consistent with experimental reaction temperatures. In addition, the majority of the rearrangements can be viewed in terms of concerted diamond–square–diamond steps and triangular face rotations.

Keywords Deltahedron · Carboranes · Icosahedral · Triangular face rotation · Diamond–square–diamond

Introduction

The roots of modern boron cluster chemistry originated in a few seminal works by Wade [1, 2], Hart and Lipscomb [3–6], and Williams [7–9]. These compounds, which are characterized by their electron deficiencies, form non-classical three-center two-electron bonds and have been the topic of numerous texts [10–14]. This leads to the very familiar deltahedron geometries for *closo*-$C_xB_{n-x}H_{n-x+2}$ with n+1 skeletal electron pairs, *nido*-$C_xB_{n-x}H_{n-x+4}$ with n+2 skeletal electron pairs, and *arachno*-$C_xB_{n-x}H_{n-x+6}$ with n+3 skeletal electron pairs, determined empirically by Wade's Rules [1, 2, 15, 16]. Although a great deal of time has been spent in comparing and contrasting carborane systems of varying size in terms of stability, rearrangement, and reactivity [7, 8, 17–23], a special effort has been expended in understanding *closo*-$B_{12}H_{12}^{2-}$, *closo*-$C_2B_{10}H_{12}$, and their respective derivatives [21, 24–29], which is due primarily to their unusually high stability. An eclectic array of mechanisms have been quite naturally suggested for the intermolecular rearrangement of *closo*-$C_2B_{10}H_{12}$, from those involving highly symmetric cubeoctahedral and anticubeoctahedral transition states to those with relatively simple triangular face rotations (TFRs) and diamond–square–diamond (DSD) steps [4, 5, 20, 25, 30–36]. Rearrangements in substituted icosahedral $C_2B_{10}H_{12}$ have been studied experimentally by way of ^{10}B-labeling, halogen substitution, methyl substitution, and even tethered linkages [3, 24, 28, 36, 37] in the hopes that the electronic structure of the cage will be preserved.

Despite previous theoretical work on the stability of large carboranes and their derivatives and the aforementioned experimental work on intermolecular rearrangements in *closo*-$C_2B_{10}H_{12}$, there has been relatively little rigorous computational work in verifying whether any of the proposed mechanisms play a role in these intermolecular rearrangement reaction pathways. The present work confirms the presence of a TFR pathway in both the carborane and the borane case.[1] Another pathway, which consists of concerted DSD steps and the opening of the cage into a pseudo-*nido* intermediate, is also described for both cases.

Methodology

The following calculations were done using the Gaussian03 program [38]. Species were optimized and vibrational frequencies were calculated at the B3LYP/6-31G(d) level, leading to their characterization as stationary points. In

Dedicated to Professor Dr. Paul von Ragué Schleyer on the occasion of his 75th birthday.

This article has already been published online first (DOI: http://dx.doi.org/10.1007/s00894-005-0039-1). Due to an oversight, this version contained several mistakes. The article is herewith republished in its entirety as an "erratum".

Electronic Supplementary Material Electronic Supplementary Material found in http://dx.doi.org/10.1007/s00894-006-0111-5

C. A. Brown · M. L. McKee (✉)
Department of Chemistry and Biochemistry,
Auburn University,
179 Chemistry Building,
Auburn, AL 36849, USA
e-mail: mckeeml@auburn.edu
e-mail: cabrown@fas.harvard.edu

[1] From this point on, carborane will be used synonymously with icosahedral $C_2B_{10}H_{12}$ and borane with icosahedral $B_{12}H_{12}^{2-}$.

addition, zero-point energies, integrated specific heat corrections at constant pressure, and entropies were calculated at this level. Once a continuous reaction pathway was determined, single-point electronic energies were calculated for the pertinent species at the B3LYP/6-311+G(2d,p) level. The enthalpies for the species at 500 and 800 K were approximated to be the same as the enthalpy at 298 K. These values were then used to determine the absolute free energy at 298, 500, and 800 K. The change in free energies at 298, 500, and 800 K for the species in the carborane rearrangement are relative to *ortho*-$C_2B_{10}H_{12}$ and, similarly, the species in the borane rearrangement are relative to $B_{12}H_{12}^{2-}$.

Results and discussion

The reaction pathways between *ortho*-, *meta*-, and *para*-$C_2B_{10}H_{12}$, and $B_{12}H_{12}^{2-}$ are shown in Figs. 1 and 2, with representative geometries in Figs. 3 and 4, respectively. At first glance, some common features between Figs. 1 and 2 should be apparent. The arrangement of the vertices and edges for both $C_2B_{10}H_{12}$ and $B_{12}H_{12}^{2-}$ are very similar (Figs. 1 and 2). Both have two distinct pathways operating the TFR pathway and the non-TFR pathway (the non-TFR pathway is actually quite complicated and cannot be succinctly described). In addition to the graphical similarities in the schemes, the representative geometries in Figs. 3 and 4 are analogs. The *ortho*- to *meta*-$C_2B_{10}H_{12}$ case mimics the *meta*- to *para*-$C_2B_{10}H_{12}$ case, which mimics the $B_{12}H_{12}^{2-}$ case. These similarities will prove to be useful when discussing the mechanisms of the pathways in detail.

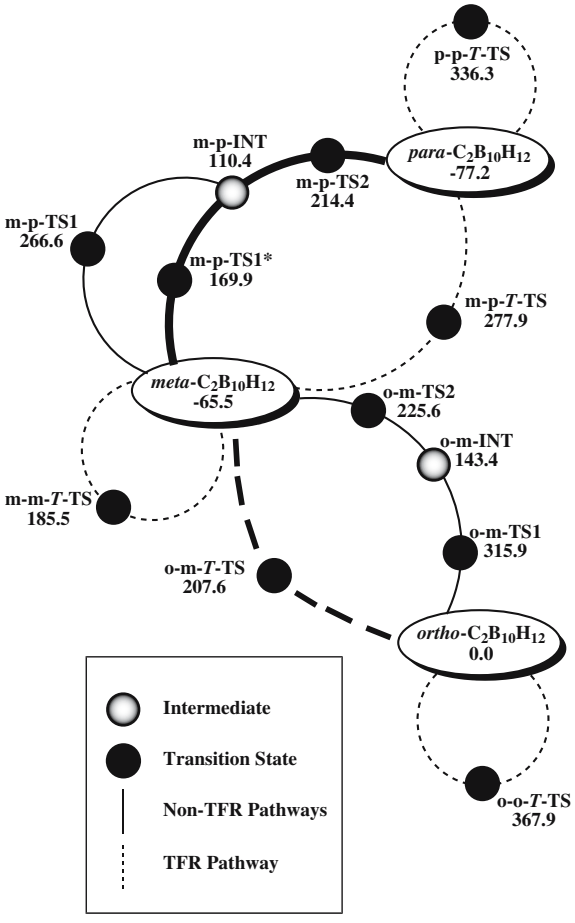

Fig. 1 Rearrangement pathways for $C_2B_{10}H_{12}$. Values indicate free energies in kilojoules per mole (kJ/mol) at 800 K. *Bold lines* (*dashed and solid*) indicate the lowest free energy pathway from *ortho*- to *meta*-$C_2B_{10}H_{12}$ (*bold and dashed*) and from *meta*- to *para*-$C_2B_{10}H_{12}$ (*bold and solid*)

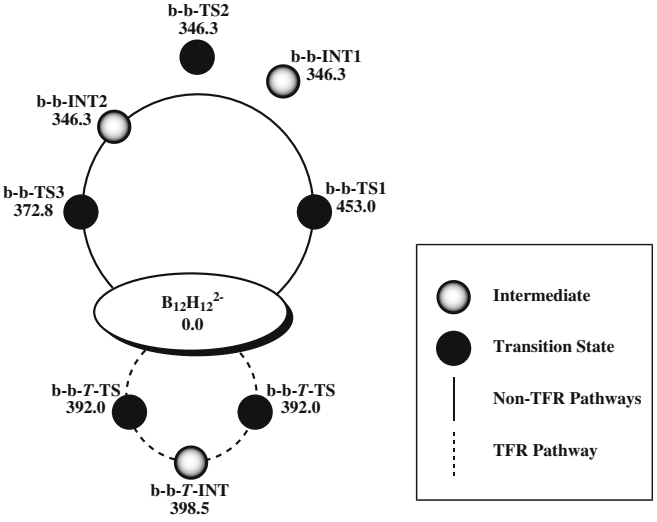

Fig. 2 Rearrangement pathways for $B_{12}H_{12}^{2-}$. Values indicate free energies in kilojoules per mole (kJ/mol) at 800 K. The stationary points *b–b*-TS2 and *b–b*-INT1 are above the curve because the free energy barrier is essentially zero, which suggests that $B_{12}H_{12}^{2-}$ is converted directly to *b–b*-INT2 (through *b–b*-TS1)

General trends

Before discussing rearrangement mechanisms, it is important to establish some confidence by way of general trends between the stabilities and geometries of the three carborane isomers. Pertinent electronic and thermodynamic data can be found in Tables 1 and 2. Notice that the ΔG (298 K) for the three isomers decreases from *ortho*- to *meta*- to *para*-$C_2B_{10}H_{12}$, which is consistent with experimental observation [39]. Furthermore, the approximate transition temperatures of 450 °C for the *ortho*- to *meta*-$C_2B_{10}H_{12}$ rearrangement and 620 °C for the *meta*- to *para*-$C_2B_{10}H_{12}$ rearrangement are qualitatively consistent with the barrier heights in Fig. 1 [39–41]. Besides trends in stability, two recent gas-phase electron diffraction (GED) studies have made it possible to compare the calculated unique bond distances in the three isomers to the

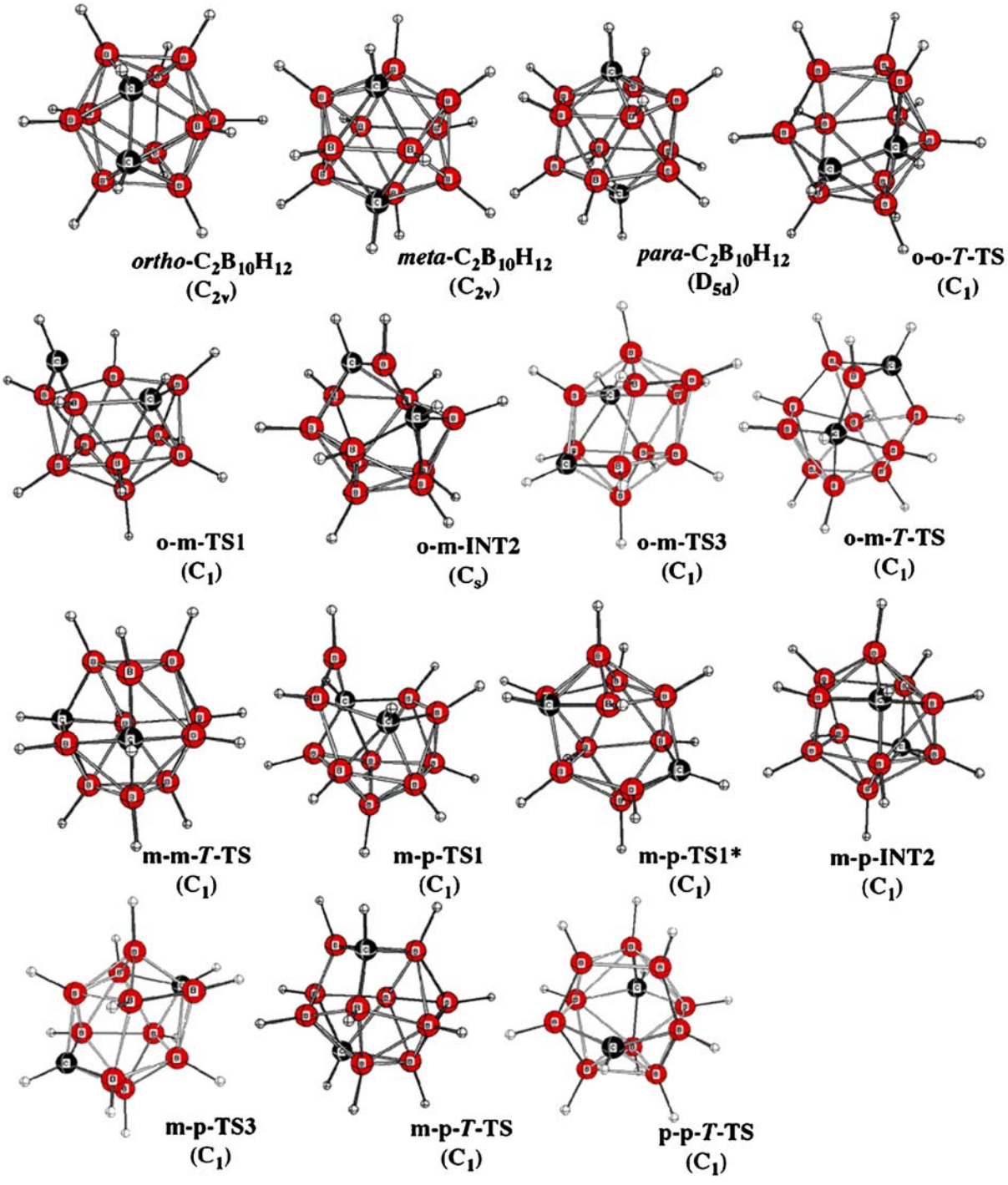

Fig. 3 Geometries for *ortho*-, *meta*-, and *para*-$C_2B_{10}H_{12}$. The nomenclature is as follows: the *first two letters* separated by a *dash* indicate which carboranes are being rearranged (e.g., m–p corresponds to a *meta* to *para* rearrangement species). An *italicized T* indicates a TFR pathway species. The *last letters* (and possible *number*) indicates the type of stationary point of the species

experimentally determined unique bond distances (see Table 3 and Fig. 5) [42, 43]. In almost all of the bonds, the difference between the calculated distance and the most recent experimentally determined distance (GED at 463 K) is around 0.01 Å.

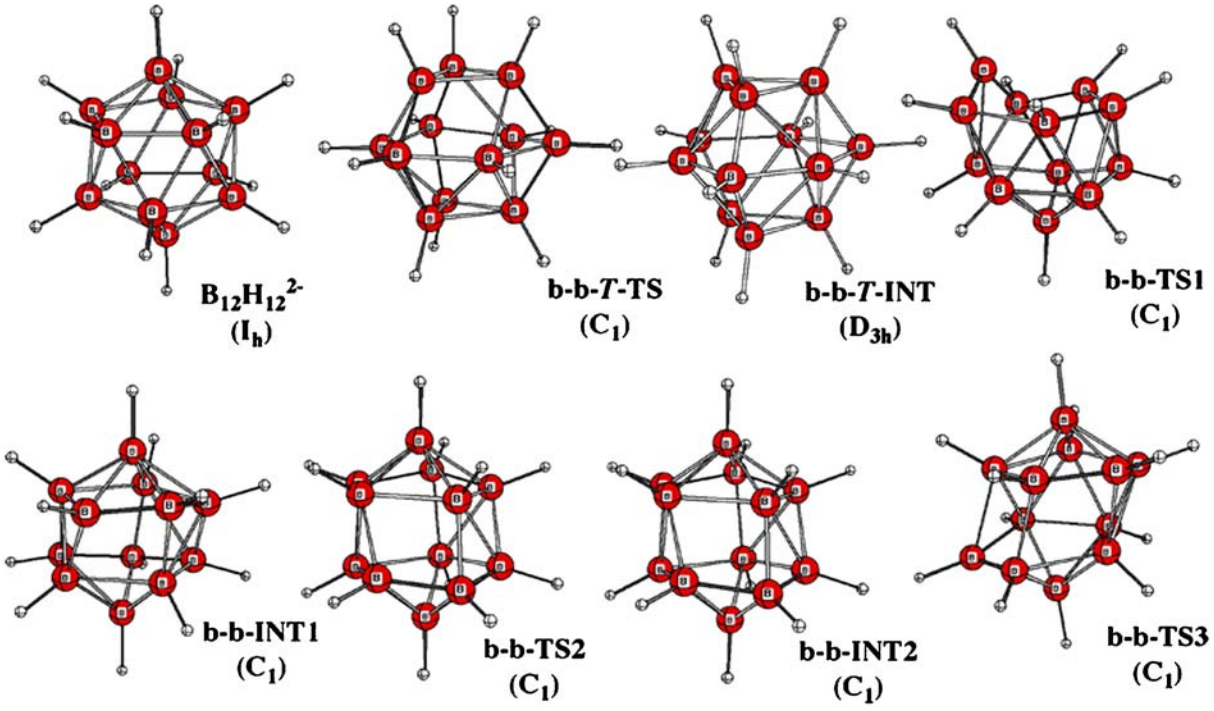

Fig. 4 Geometries of $B_{12}H_{12}{}^{2-}$ species. The nomenclature system is analogous to the carborane case. Consult Fig. 3 for a description

Table 1 Total electronic energies (in hartrees), zero-point energies (kJ/mol), heat capacity corrections to 298 K, and entropies (J/mol K) for species on the $C_2B_{10}H_{12}$ and $B_{12}H_{12}{}^{2-}$ potential energies surfaces

Structures	Total energy	Zero-point energy	∫ Cp	Entropy
ortho-$C_2B_{10}H_{12}$	−332.17455	466.1	22.7	347.1
meta-$C_2B_{10}H_{12}$	−332.20059	468.0	22.4	345.5
para-$C_2B_{10}H_{12}$	−332.20500	468.0	22.4	345.7
o–m-TS1	−332.04031	445.7	26.6	372.2
o–m-INT	−332.10921	455.1	26.8	373.7
o–m-TS2	−332.07899	451.5	25.4	363.8
o–m-T-TS	−332.08224	448.5	26.7	373.5
o–o-T-TS	−332.01780	444.1	27.6	380.3
m–m-T-TS	−332.09144	449.5	26.7	372.2
m–p-TS1	−332.06051	448.2	26.3	370.2
m–p-TS1*	−332.10091	452.5	25.1	362.4
m–p-INT	−332.12258	455.5	26.6	371.5
m–p-TS2	−332.08274	451.5	25.6	365.8
*m–p-**T***-TS	−332.05341	446.7	27.3	378.8
p–p-T-TS	−332.03032	444.5	27.7	379.4
$B_{12}H_{12}^{2-}$	−305.77394	439.1	23.1	348.7
b–b-T-TS	−305.60815	418.6	28.3	383.6
b–b-T-INT	−305.60974	419.7	29.6	373.2
b–b-TS1	−305.58691	419.4	27.4	377.1
b–b-INT1	−305.63168	423.9	26.0	367.4
b–b-TS2	−305.63167	423.9	26.0	367.4
b–b-INT2	−305.63167	423.9	26.0	367.5
b–b-TS3	−305.61911	422.4	26.6	374.5

Table 2 Relative enthalpies (kJ/mol), entropies (J/K·mol), and free energies (kJ/mol) for species on the $C_2B_{10}H_{12}$ and $B_{12}H_{12}^{2-}$ potential energy surfaces

Structures	ΔH (0 K)	ΔH (298 K)	ΔS	ΔG (298 K)	ΔG (500 K)	ΔG (800 K)
ortho-$C_2B_{10}H_{12}$	0.0	0.0	0.0	0.0	0.0	0.0
meta-$C_2B_{10}H_{12}$	−66.5	−66.8	−1.5	−66.3	−66.0	−65.5
para-$C_2B_{10}H_{12}$	−78.0	−78.3	−1.4	−77.9	−77.6	−77.2
o–m-TS1	332.1	336.0	25.1	328.5	323.4	315.9
o–m-INT	160.6	164.7	26.6	156.8	151.4	143.4
o–m-TS2	236.3	239.0	16.7	234.0	230.6	225.6
o–m-T-TS	224.7	228.8	26.4	220.9	215.5	207.6
o–o-T-TS	389.6	394.5	33.3	384.6	377.9	367.9
m–m-T-TS	201.6	205.6	25.1	198.1	193.1	185.5
m–p-TS1	281.6	285.1	23.1	278.2	273.6	266.6
m–p-TS1*	179.8	182.2	15.4	177.6	174.5	169.9
m–p-INT	125.9	129.9	24.4	122.6	117.7	110.4
m–p-TS2	226.5	229.4	18.7	223.8	220.0	214.4
m–p-T-TS	298.7	303.3	31.7	293.8	287.4	277.9
p–p-T-TS	357.1	362.1	32.3	352.5	346.0	336.3
$B_{12}H_{12}^{2-}$	0.0	0.0	0.0	0.0	0.0	0.0
b–b-T-TS	414.7	419.9	34.9	409.5	402.5	392.0
b–b-T-INT	411.6	418.2	24.5	410.8	405.9	398.5
b–b-TS1	471.4	475.7	28.4	467.2	461.5	453.0
b–b-INT1	358.3	361.3	18.7	355.7	351.9	346.3
b–b-TS2	358.3	361.3	18.7	355.7	351.9	346.3
b–b-INT2	358.3	361.3	18.8	355.7	351.9	346.3
b–b-TS3	389.8	393.4	25.8	385.7	380.5	372.8

Ortho- to *meta*-carborane rearrangement[2]

TFR pathway

Figure 6 illustrates the *ortho*- to *meta*-$C_2B_{10}H_{12}$ TFR mechanism where the structures of the stationary points are similar to those in the *ortho*-$C_2B_{10}H_{12}$ to *ortho*-$C_2B_{10}H_{12}$ degenerate TFR, the *meta*-$C_2B_{10}H_{12}$ to *para*-$C_2B_{10}H_{12}$ TFR, and the borane TFR rearrangement.[3] The left column in Fig. 6 displays the geometric progression through the reaction and the right column shows a two-dimensional projection of the pertinent atoms and bonds of the corresponding geometry on the left. As can be seen in the left column, a TFR acts by taking an equilateral triangle of three atoms, lifting them up slightly, rotating them by 120 ° (counter-clockwise in this case), and lowering them back down. The projective graphs display unequivocally that the mechanism is, in fact, a sequence of concerted diamond–square–diamonds. The transition state graph corresponding to *o–m-T*-TS shows the three simultaneous square faces.

Non-TFR pathway

Figure 7 illustrates the non-TFR mechanism. The first step in this mechanism is for one of the *ortho*-$C_2B_{10}H_{12}$ carbons, situated at the apex of a pentagonal cap, to break three of its bonds, while performing a DSD transition on the lower diamond. The square face in the DSD transition can be seen in the lower part of the graph corresponding to *o-m*-TS1. As the carbon migrates and forms the bond in the DSD, the species approaches a pseudo-*nido* geometry, which is displayed graphically in brackets. This geometry, in which the carbon lies approximately in a hexagonal plane, is never realized because other stabilizing forces exert themselves and propel the species towards the geometry in *o-m*-INT. The geometry displays two pentagonal faces in lieu of the hexagonal face of the pseudo-*nido* geometry. The last transition state *o-m*-TS2 is due to two adjacent DSD transitions on the opposite side of the cluster. In one direction, the species minimizes to *o-m*-INT. In the other direction, the molecule minimizes to *meta*-$C_2B_{10}H_{12}$.

Meta- to *para*-carborane rearrangement

TFR pathway

See "TFR pathway" subsection under "Ortho- to meta-carborane rearrangement".

[2] David Wales has two examples of carborane rearrangements that illustrate the necessary movement: (1) rearrangement from the icosahedral 1,2-carborane to a higher energy C_S isomer (http://www.ch.cam.ac.uk/SGTL/teach/djw1.html) and (2) rearrangement from the 1,7-icosahedral carborane to a higher energy isomer based on an anticuboctahedron (http://www.ch.cam.ac.uk/SGTL/teach/djw2.html).

[3] All of these pathways operate in essentially the same manner, except for slight deviations in geometry due to juxtaposition of boron with carbon and vice versa.

Table 3 Comparison of calculated distances [B3LYP/6-31G(d)] with distances from two gas-phase electron diffraction studies for *ortho*-, *meta*-, and *para*-$C_2B_{10}H_{12}$

Bond	B3LYP/6-31G(d)	GED [42]	GED [43]
ortho-$C_2B_{10}H_{12}$			
C(1)–C(2)	1.625	1.624(8)	1.653(49)
C(1)–B(3)	1.720	1.734(7)	1.711(14)
C(1)–B(4)	1.700	1.700(6)	1.711(14)
B(3)–B(4)	1.780	1.788(6)	1.802(13)
B(4)–B(5)	1.786	1.794(8)	1.802(13)
B(3)–B(8)	1.765	1.774(9)	1.789(9)
B(5)–B(9)	1.778	1.787(6)	1.789(9)
B(7)–B(8)	1.781	1.796(6)	1.789(9)
B(8)–B(9)	1.793	1.808(8)	1.789(9)
B(9)–B(12)	1.784	1.787(9)	1.789(9)
meta-$C_2B_{10}H_{12}$			
C(1)–B(2)	1.694	1.678(5)	1.720(9)
C(1)–B(4)	1.715	1.730(4)	1.720(9)
C(1)–B(5)	1.712	1.704(8)	1.720(9)
B(2)–B(3)	1.789	1.786(9)	1.831(52)
B(2)–B(6)	1.768	1.771(6)	1.791(15)
B(4)–B(5)	1.783	1.801(5)	1.791(15)
B(4)–B(9)	1.781	1.780(6)	1.817(13)
B(5)–B(9)	1.778	1.783(6)	1.817(13)
B(4)–B(8)	1.771	1.778(9)	1.817(13)
B(9)–B(10)	1.793	1.795(9)	1.817(13)
C(1)···C(7)	2.608	2.575(9)	
para-$C_2B_{10}H_{12}$			
C–B	1.708	1.698(3)	1.710(11)
B–B tropical	1.790	1.784(1)	1.792(7)
B–B meridianal	1.767	1.774(4)	1.772(13)
C(1)···C(12)	3.057	3.029(5)	3.05(5)

Non-TFR pathway

The non-TFR mechanism for the *meta*- to *para*-rearrangement (Fig. 8) mimics the *ortho*- to *meta*-$C_2B_{10}H_{12}$ rearrangement except that there is a second possible transition state *m–p*-TS1*, which is lower in energy than the analogous *ortho*- to *meta*-$C_2B_{10}H_{12}$ transition state (*m–p*-TS1, Table 1). The structural change from *meta*-$C_2B_{10}H_{12}$ to *m–p*-TS1 is exactly the same as in the *ortho*- to *meta*-$C_2B_{10}H_{12}$ case, except that only a boron vertex moves from the apex of a pentagonal cap opening a face in the cluster. Just as with the *ortho*- to *meta*-$C_2B_{10}H_{12}$ rearrangement, a "*nido*" geometry is never reached, leading instead to *m–p*-INT. The more thermodynamically favorable pathway is through *m–p*-TS1* which can be described as two adjacent concerted DSD steps. The second half of the rearrangement is analogous to the *ortho*-$C_2B_{10}H_{12}$ to *meta*-$C_2B_{10}H_{12}$ rearrangement: two concerted adjacent DSD steps occur on the opposite side of the cluster (see *m–p*-TS2) and *para*-$C_2B_{10}H_{12}$ results.

Borane rearrangement

TFR pathway

See "TFR pathway" subsection under "Ortho- to meta-carborane rearrangement". There is one exception in the $B_{12}H_{12}^{2-}$ case. There is a D_{3h} intermediate *b–b-T*-INT that is lower than *b–b-T*-TS in enthalpy at 298 K by 1.7 kJ/mol. When entropic effects are taken into account, the intermediate *b–b-T*-INT is actually higher in free energy at 298, 500, and 800 K.

Non-TFR pathway

Figure 9 illustrates the non-TFR mechanism in the $B_{12}H_{12}^{2-}$ rearrangement. The first transition state *b–b*-TS1 is essentially the same as *o–m*-TS1 and *m–p*-TS1 except that there are no carbon atoms present. A boron atom located at

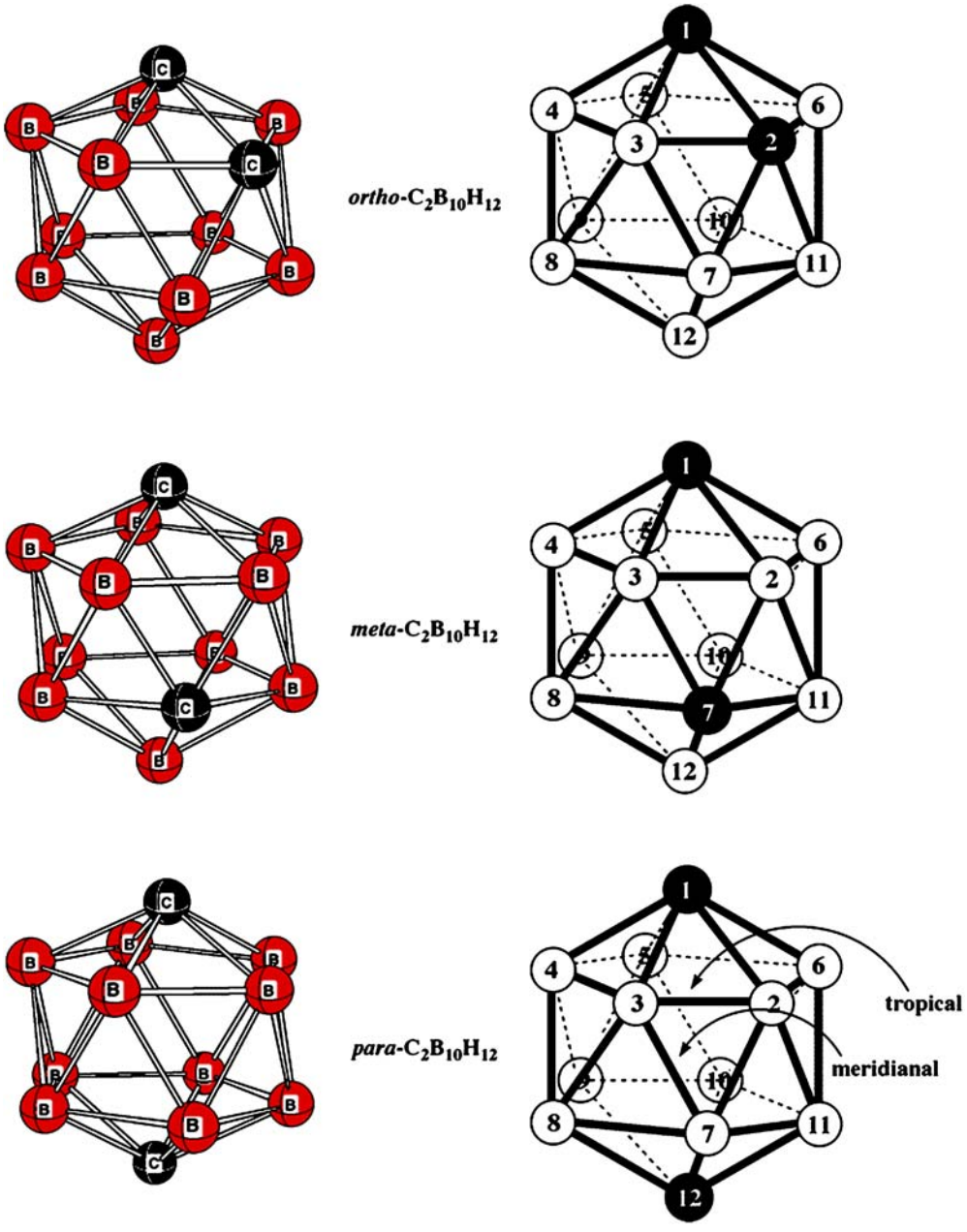

Fig. 5 Numbering system with respective geometries for Table 3

the apex of a pentagonal cap migrates, breaking three bonds, and performs a DSD step on the lower diamond. The geometry again progresses towards a pseudo-*nido* geometry but does not quite achieve it. Another bond begins to form, which acts to prevent the cluster from opening, resulting in *b*–*b*-INT1. An interesting feature of the pathway is that there is an additional minimum (*b*–*b*-TS2) and transition state (*b*–*b*-INT1) along the reaction pathway that disappear when zero-point corrections are included. From *b*–*b*-TS2, two adjacent concerted DSD steps are needed to reach *b*–*b*-TS3 which then leads directly to icosahedral $B_{12}H_{12}^{2-}$.

The free energy of activation in the gas phase for rearrangement of the boron vertices at 800 K is 398.5 kJ/mol via *b*–*b*-*T*-INT (Fig. 2). The free energy barrier is much higher than calculated for rearrangement in the isoelectronic carboranes (Fig. 1). In fact, the barrier is higher than for fragmentation of a B–H bond, which implies that $B_{12}H_{12}^{2-}$ should undergo decomposition rather than rearrangement. In a recent study of the boron hydride monoanions, $B_{12}H_{12}^{2-}$ was determined to be the smallest boron hydride dianion with a positive adabatic ionization potential [22]. It is still unlikely that both electrons would remain attached at elevated temperatures.

Experimental verification

There is one very interesting anomaly that emerges with respect to carborane rearrangements. The lowest free

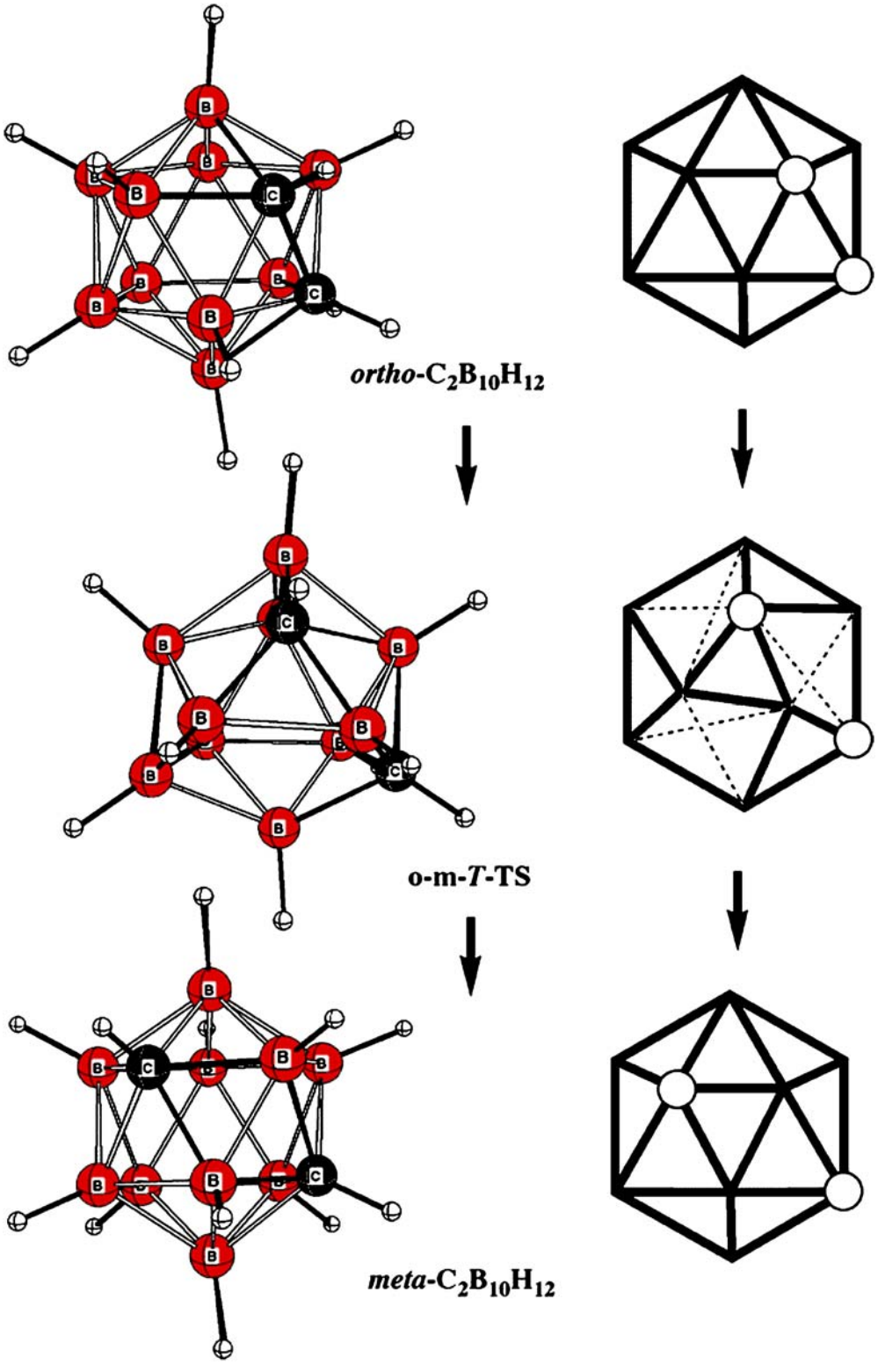

Fig. 6 A localized graphical picture that describes the progression of the TFR pathway. The *ortho*- to *meta*-$C_2B_{10}H_{12}$ TFR pathway is shown

energy carborane barrier is a degenerate rearrangement *meta*- to *meta*-$C_2B_{10}H_{12}$, which is 185.5 kJ/mol at 800 K. This process may prove useful in rationalizing products obtained from rearrangement of the substituted carborane. In addition, because the barrier is lower than the barrier for rearrangement to *ortho*- and *para*-$C_2B_{10}H_{12}$, if one were able to synthesize a substituted *meta*-$C_2B_{10}H_{12}$ with a methyl group on a boron atom adjacent to carbon, then, at a moderate temperature, one would expect to see migration of the methyl group to a boron position non-adjacent to carbon. We offer this prediction as a means of testing the rearrangement mechanism in the gas phase.

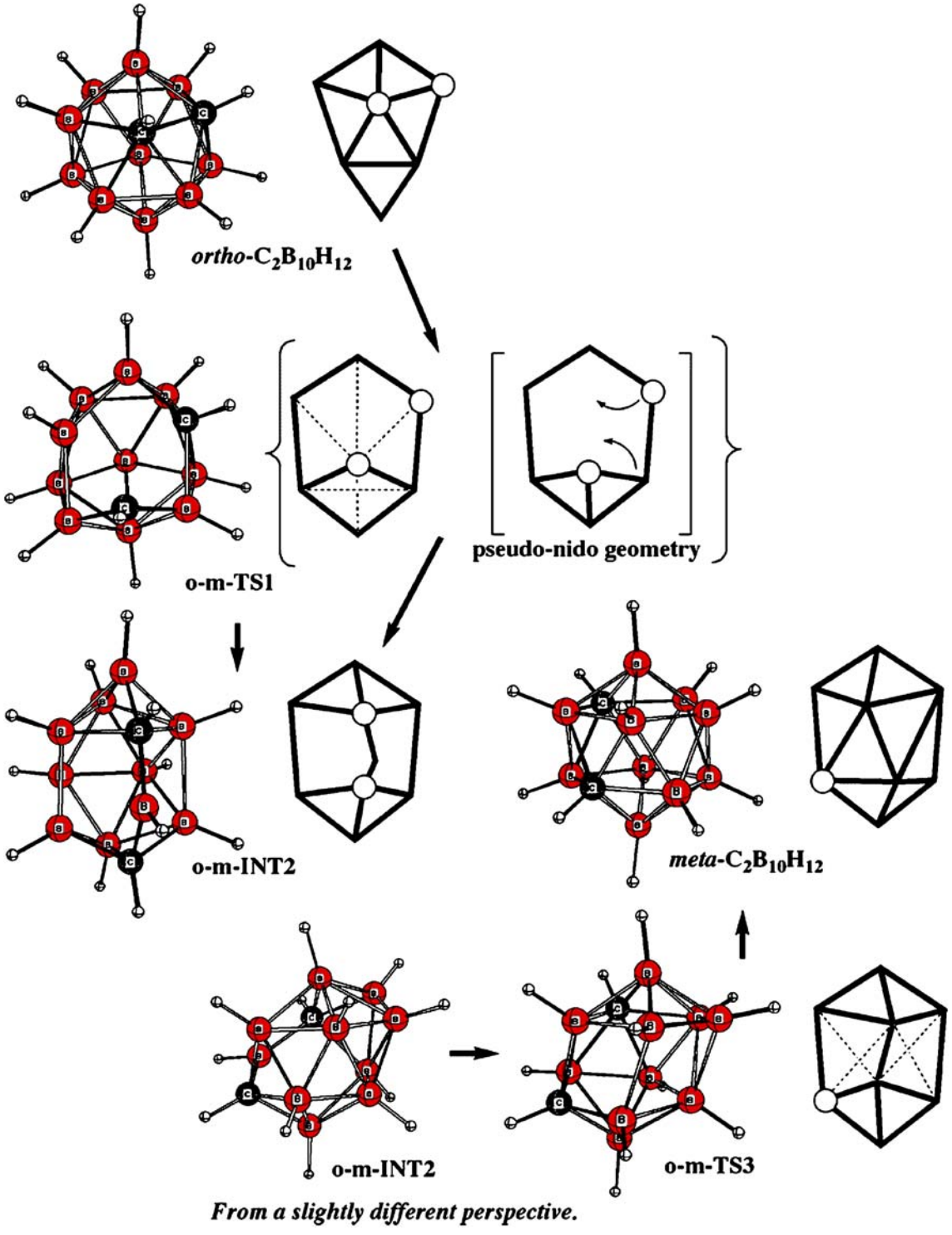

Fig. 7 The *ortho*- to *meta*-$C_2B_{10}H_{12}$ non-TFR rearrangement pathway

Conclusion

The rearrangement mechanism in $C_2B_{10}H_{12}$ and $B_{12}H_{12}^{2-}$ has been explored using density functional theory methods. From *ortho*-$C_2B_{10}H_{12}$, the lowest free energy pathway to *meta*-$C_2B_{10}H_{12}$ is via a triangular-face-rotation mechanism with a barrier of 207.6 kJ/mol. From *meta*- to *para*-$C_2B_{10}H_{12}$, the lowest-energy rearrangement mechanism is non-TFR which might loosely be described as a *closo* to *nido* to *closo* mechanism as the transition state is much more open than the reactant or product. The free energy barrier is 279.9 kJ/mol, 72.3 kJ/mol lower in free energy

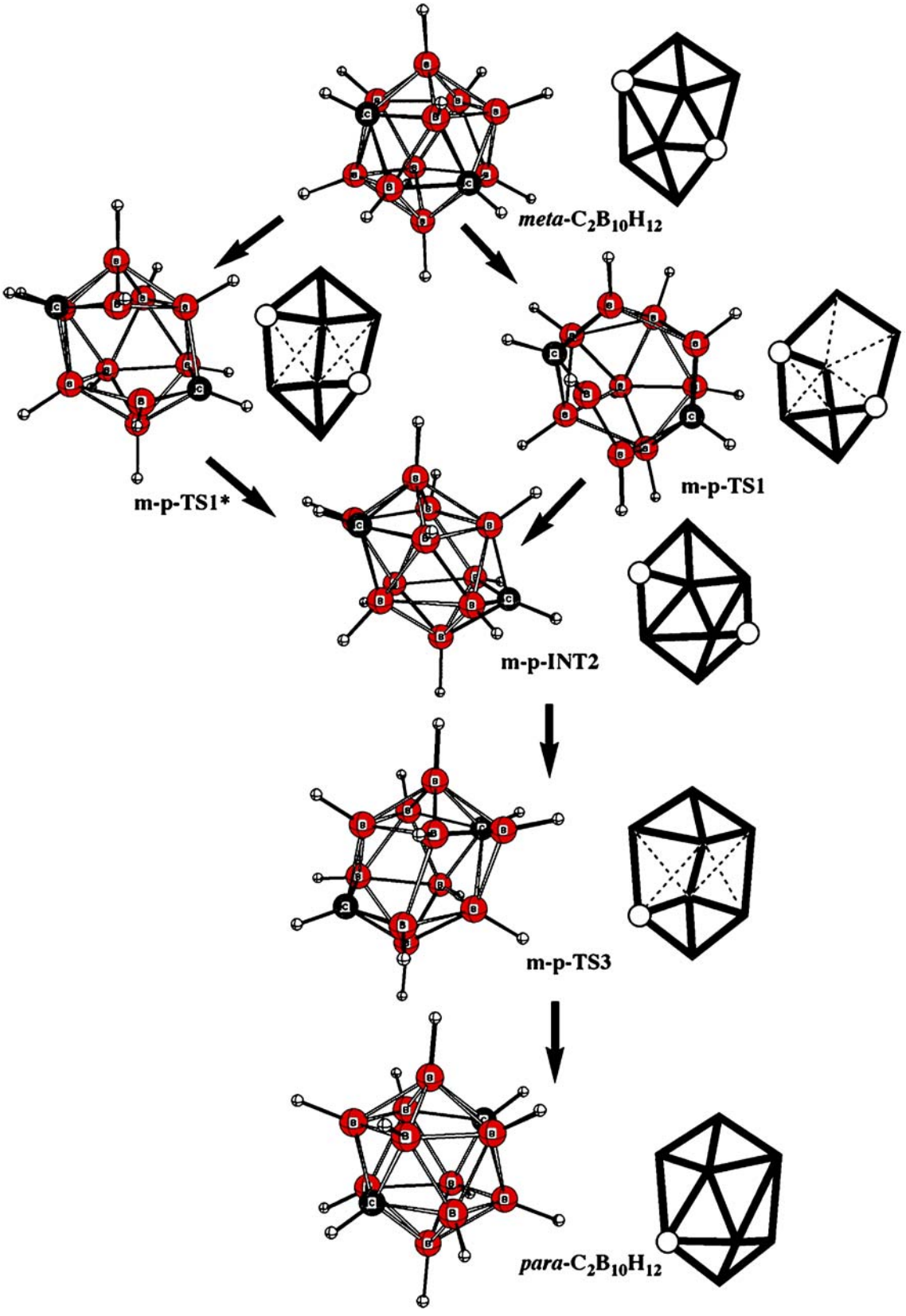

Fig. 8 The *meta*- to *para*-$C_2B_{10}H_{12}$ non-TFR rearrangement pathway

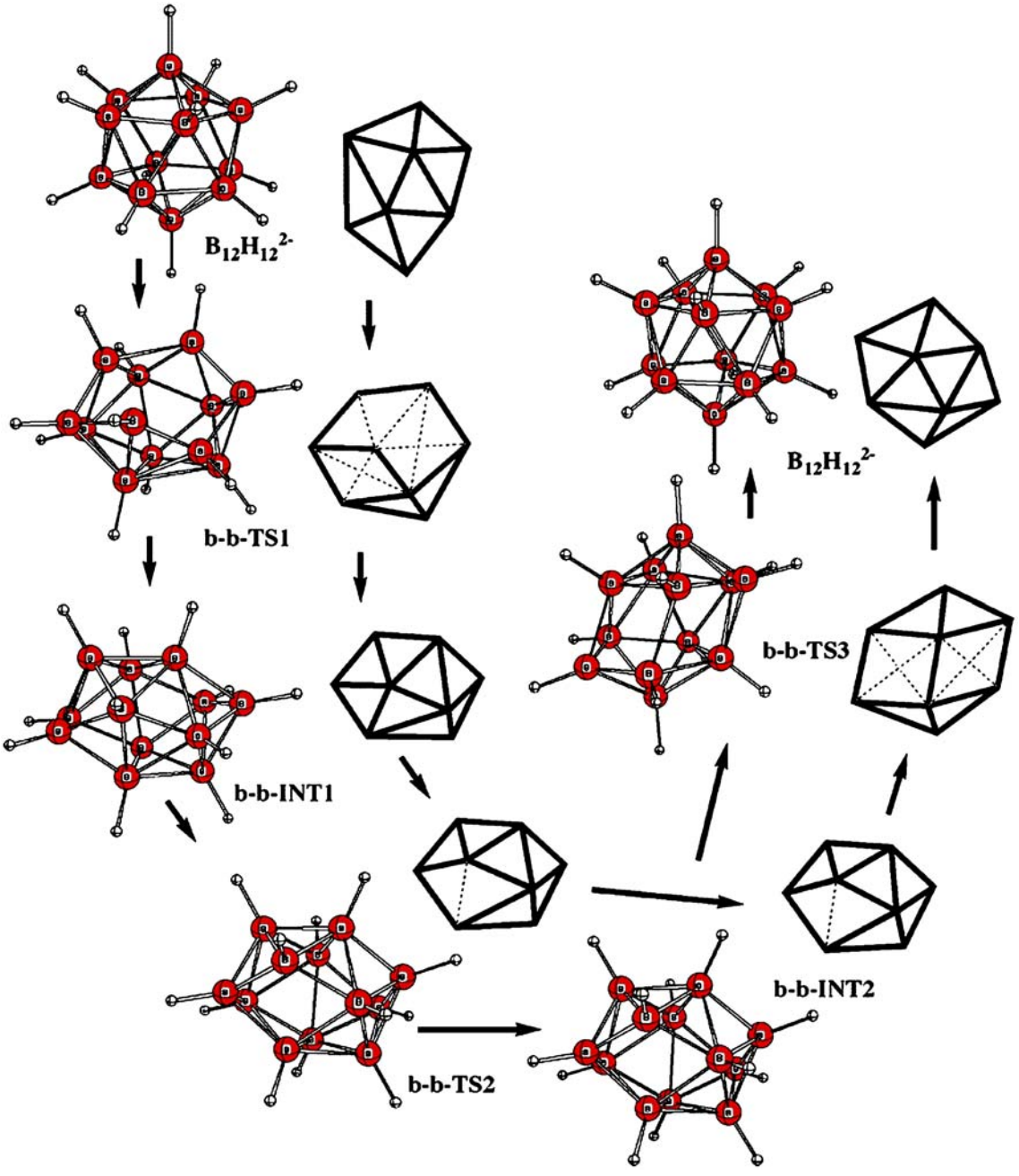

Fig. 9 The $B_{12}H_{12}^{2-}$ to $B_{12}H_{12}^{2-}$ non-TFR rearrangement pathway

than the *ortho* to *meta* process. The rearrangement of $B_{12}H_{12}^{2-}$, which would scramble labeled vertices, has a free energy barrier of 398.5 kJ/mol. For $B_{12}H_{12}^{2-}$, the preferred process in the gas phase would be to emit an electron or cleave a B–H bond.

Acknowledgements We acknowledge the Alabama Supercomputer Center for providing time on their SGI Altix 350. C. A. B. would like to thank the College of Science and Mathematics at Auburn University for an undergraduate research fellowship. Above all, we appreciate the numerous contributions that Prof. Schleyer has made to chemistry.

References

1. Wade K (1976) Adv Inorg Chem Radiochem 18:1–66
2. Wade K (1971) Chem Commun 1:792–793
3. Hart HV, Lipscomb WN (1973) Inorg Chem 12:2644–2649
4. Hart HV, Lipscomb WN (1969) J Am Chem Soc 91:771–772
5. Lipscomb WN (1966) Science 153:373–378
6. Lipscomb WN (1959) Adv Inorg Chem Radiochem 1:117–156
7. Williams RE (1971) Inorg Chem 10:210–214
8. Williams RE, Gerhart FJ (1965) J Am Chem Soc 87: 3513–3515
9. Williams RE (1976) Adv Inorg Chem Radiochem 18:67–142
10. Driess M, Nöth H (eds) (2004) Molecular clusters of the main group elements. Wiley-VCH Verlag GmbH KGaA, Weinheim
11. Grimes RN (1970) Carboranes. Academic, New York

12. Lipscomb WN (1963) Boron hydrides. Benjamin, New York
13. Mingos DMP, Wales DJ (1990) Introduction to cluster chemistry. Prentice Hall, New York
14. Mutterties EL, Knoth WH (1968) Polyhedral boranes. Marcel Dekker, New York
15. Fox MA, Wade K (2003) Pure Appl Chem 75:1315–1323
16. Kiani FA, Hofmann M (2004) Inorg Chem 43:8561–8571
17. Casanova J (ed) (1998) The borane, carborane, carbocation continuum. Wiley, New York
18. Ceulemans A, Goijens G, Nguyen MT (1994) J Am Chem Soc 116:9395–9396
19. Deng L, Chan H, Xie Z (2005) Angew Chem Int Ed 44:2–5
20. Kaczmarcyzk A, Dobrott RD, Lipscomb WN (1962) Proc Natl Acad Sci U S A 48:729–733
21. Laromaine A, Teixidor F, Viñas C (2005) Angew Chem Int Ed 44:2–4
22. McKee ML, Wang Z, Schleyer PvR (2000) J Am Chem Soc 122:4781–4793
23. McKee ML (1992) J Am Chem Soc 114:879–881
24. Barnett-Thamattoor L, Wu JJ, Ho DM, Jones M Jr (1996) Tetrahedron Lett 37:7221–7224
25. Gimarc BM, Warren DS, Ott JJ, Brown C (1991) Inorg Chem 30:1598–1605
26. McKee ML (1994) J Phys Chem 98:13243–13248
27. McKee ML (1992) J Am Chem Soc 114:5856–5858
28. Wong HS, Lipscomb WN (1975) Inorg Chem 6:1350–1357
29. Ye Q, Li J, Jones M Jr, Wu H, Mckee ML, Shevlin PB (2002) Tetrahedron Lett 43:735–736
30. Gimarc BM, Zhao M (1996) Inorg Chem 35:825–834
31. Johnson BFG (1986) Chem Commun 1:27–30
32. Roberts YV, Johnson BFG (1994) J Chem Soc Dalton Trans 5:759–766
33. Wales DJ, Mingos DMP, Zhenyang L (1989) Inorg Chem 28:2754–2764
34. Wales DJ, Mingos DMP (1989) Polyhedron 8:1933–1938
35. Wales DJ, Stone AJ (1987) Inorg Chem 26:3845–3850
36. Wu S, Jones M Jr (1989) J Am Chem Soc 111:5373–5384
37. Edvenson GM, Gaines DF (1990) Inorg Chem 29:1210–1216
38. Frisch MJ, Trucks GW, Schlegel HB, Scuseria GE, Robb MA, Cheeseman JR, Montgomery JA Jr, Vreven T, Kudin KN, Burant JC, Millam JM, Iyengar SS, Tomasi J, Barone V, Mennucci B, Cossi M, Scalmani G, Rega N, Petersson GA, Nakatsuji H, Hada M, Ehara M, Toyota K, Fukuda R, Hasegawa J, Ishida M, Nakajima T, Honda Y, Kitao O, Nakai H, Klene M, Li X, Knox JE, Hratchian HP, Cross JB, Bakken V, Adamo C, Jaramillo J, Gomperts R, Stratmann RE, Yazyev O, Austin AJ, Cammi R, Pomelli C, Ochterski JW, Ayala PY, Morokuma K, Voth GA, Salvador P, Dannenberg JJ, Zakrzewski VG, Dapprich S, Daniels AD, Strain MC, Farkas O, Malick DK, Rabuck AD, Raghavachari K, Foresman JB, Ortiz JV, Cui Q, Baboul AG, Clifford S, Cioslowski J, Stefanov BB, Liu G, Liashenko A, Piskorz P, Komaromi I, Martin RL, Fox DJ, Keith T, A*l*-Laham MA, Peng CY, Nanayakkara A, Challacombe M, Gill PMW, Johnson B, Chen W, Wong MW, Gonzalez C, Pople JA (2004) Gaussian, Wallingford, CT
39. Mutterties EL (1975) Boron hydride chemistry. Academic, New York
40. Grafstein D, Dvorak J (1963) Inorg Chem 2:1128–1133
41. Papetti S, Heying TL (1964) J Am Chem Soc 86:2295
42. Turner AR, Robertson HE, Borisenko KB, Rankin DWH, Fox MA (2005) J Chem Soc Dalton Trans 7:1310–1318
43. Bohn RK, Bohn MD (1971) Inorg Chem 10:350–355